LaNi$_{0.6}$Fe$_{0.4}$O$_3$ as Cathode Contacting Material:
Effect on Anode Supported Cell Performances

R. Spotorno[a], P. Piccardo[a], R. Costa[b], F. Han[b], G. Schiller[b]

[a] Department of Chemistry and Industrial Chemistry, University of Genoa, Genoa, Italy
[b] German Aerospace Center, Stuttgart, Germany

In this work, LaNi$_{0.6}$Fe$_{0.4}$O$_3$ (LNF) powders have been synthesized by sol-gel methods and used to prepare a contacting paste. A testing setup, developed to test anode-supported cells with different contacting geometries, has been used to investigate the effect of LNF contacting paste between the cathode and the current collector. The cell performances were comparable to those measured using a state-of-the-art La$_{0.6}$Sr$_{0.4}$Co$_{0.2}$Fe$_{0.8}$O$_3$ (LSCF) contacting paste, however, showing better stability under electric load. Cell performances have been investigated by means of current-voltage curves. Electrochemical impedance spectroscopy has been used to distinguish the loss contribution within the investigated system and to measure its evolution over time. The performances evolution was confirmed by microstructural changes and migration of elements characterized post-experiment by means of scanning electron microscopy-energy dispersive X-ray and X-ray diffraction techniques.

Introduction

In planar solid oxide fuel cell (SOFC) stacks, ohmic losses are introduced at the interface between the electrodes and current collectors, especially in the cathodic compartments, due to the contact inhomogeneity. Such losses are usually responsible for the major performance decrease of the stack limiting its power output (1).

The porosity of the electrodes and geometrical issues linked to the shape of interconnects are factors resulting in the reduction of the contact surface between such components. Contacting layers are often applied between the cathode and the interconnect in order to minimize the influence of such issues ensuring a uniform current collection from the electrode (2,3) during the operation of the cells, increasing the performances in terms of power output and mitigating their degradation rate (4).

Contacting materials have no direct involvement in the electrochemical reactions; therefore, they are not required to be catalytically active or ionic conductive. However, they should have high electronic conductivity and suitable coefficient of thermal expansion (CTE) matching the adjacent cell components. Their initial sintering temperature should be below 1000°C to avoid dedicated curing treatment that could damage the metallic parts of the stack. Additionally, contacting materials must be chemically stable at the SOFC operating conditions avoiding reactions with the neighboring materials and the formation of detrimental phases (5-7). To meet such

conditions, the same perovskite materials constituting the electrodes are often applied as contacting materials. $LaNi_{0.6}Fe_{0.4}O_3$ is already known as suitable contacting material for SOFC cathodes having a good CTE, chemical stability and an electrical conductivity higher than the state-of-the-art cathodes (8,9).

In this work specifically, we further investigated LNF materials. Powders were first synthesized by sol-gel methods to prepare a contacting paste. A testing setup, developed to test anode-supported cells with different contacting geometries, has been used to investigate the effect of LNF contacting paste between the cathode and the current collector. The performance of the assembly cell + contact layer + interconnect has been investigated by means of current-voltage curves. Microstructural changes and migration of elements have been characterized post-experiment by means of scanning electron microscopy-energy dispersive X-ray (SEM-EDX) and X-ray diffraction techniques (XRD).

Materials and Methods

LNF powders were synthesized by sol-gel method mixing, in stoichiometric amounts, $La(NO_3)_3*6H_2O$, $Ni(NO_3)_2*6H_2O$ and $Fe(NO_3)_2*9H_2O$ (Fluka Chemika, Switzerland, purity 99%) in deionized water. An excess (3.3 mol/mol) of citric acid (Sigma Aldrich, Germany, purity 98%) was added to act as chelant. The choice of nitrates was driven by their low decomposition temperatures (below 400°C). The solution was heated at 120°C until viscous gels were obtained. A firing treatment in air at 600°C for 1 hour was performed in order to obtain a xerogel. Powders, obtained by grinding the xerogel in a mortar, were annealed in air for 4 hours at various temperatures in the range 800-1100°C. Calcined powders were grinded and ball-milled for 70 hours and then characterized by XRD using a D8 Discover GADDS X-ray diffractometer (Bruker, Germany), equipped with a VÅNTEC-2000 area detector. Such characterization was carried out to investigate the effect of annealing temperature on the right phase formation and the presence of any contamination introduced during the whole production process.

The synthesized LNF and commercially available LSCF (FCM, USA) were mixed with the ink vehicle (94 wt% terpineol, 6 wt% polyethylene glycol) and homogenized in an Exakt 80E three roll mill (Exakt Advanced Technologies GmbH, Norderstedt, Germany) to form a contacting paste (60 wt% powder, 40 wt% solvent).

Porous pellets were prepared by drying contacting inks in a die and then sintering the greens in static air at 1200°C for 4 hours to obtain samples for dilatometry measurements. The CTE was measured using a DIL 402 C (Netzsch-Gerätebau GmbH) from room temperature to 900°C in air with a heating rate of 5°C min^{-1}.

Commercially available anode-supported cells (ASC) manufactured by CeramTec AG (Marktredwitz, Germany) were tested with LNF and LSCF contacting pastes at the cathode side. Pastes were brushed over the electrode to obtain homogeneous layers. Cells consisted of a 50 mm x 50 mm Ni/8YSZ-cermet anode (where 8YSZ: 8 mol% Y_2O_3 doped ZrO_2), a 50 mm x 50 mm 8YSZ electrolyte with GDC ($Ce_{0.8}Gd_{0.2}O_{2-\delta}$) interlayer at the cathode side followed by a LSCF ($La_{0.6}Sr_{0.4}Co_{0.2}Fe_{0.8}O_{3-\delta}$) 40 mm x 40 mm cathode. Metallic meshes (Heraeus Deutschland GmbH & Co. KG) with a wire diameter of 0.04

mm, mesh width of 0.12 mm and 3600 meshes per cm^2 were used as current collector between the cell and the electronic characterization devices at both the anode and the cathode side. On both sides Pt meshes were spot-welded with the platinum wires used as potential probes and current carriers. The current collector at the cathode side and a nickel mesh at the anode were placed between these meshes and the electrodes. The use of a Ni mesh at the anode was intended to avoid alloying between the platinum contacts and the nickel contained in the electrode.

The cathode current collector was produced by a stamping process (Graebner Maschinentechnik GmbH & Co. KG, Germany) using Crofer 22 APU plates 0.5 mm thick (ThyssenKrupp VD). The obtained interconnects were square-shaped corrugated 30 mm × 30 mm plates characterized by an asymmetric design with 3.5 mm wide air channels and 0.5 mm wide contact ribs.

Tests on ASCs were performed using a dedicated setup already described in a previous study (10) designed to host the interconnect at the cathode side as current collector. In this way, it was possible to test the influence of contacting on the cell performances.

Each cell was heated up to 900°C with a ramp speed of 5°C min^{-1} in flowing dry air at the cathode side (0.5 Nlmin^{-1}) and dry nitrogen at the anode (0.5 Nlmin^{-1}). At 900°C the anode reduction was performed gradually introducing hydrogen in the nitrogen flow. The anode gas flow composition was gradually turned to 1 Nl min^{-1} of 3% wet hydrogen while the air flow at the cathode was increased to 1 Nl min^{-1}. After 1 hour in such conditions, the furnace temperature was lowered to 750°C to start the cell performance evaluation by current-potential (I-V) curves and Electrochemical Impedance Spectroscopy (EIS) measurements. The electrochemical characterization was carried out using an Electrochemical Workstation IM6 (Zahner-Elektrik GmbH & Co. KG, Kronach, Germany).

I-V curves were measured applying an increasing current load by steps of 0.125 mA cm^{-2} up to cell voltages not below 0.6 V.

EIS spectra were recorded in the frequency range 0.1 Hz–100 kHz and deconvoluted using a Complex Non-Linear Regression Least-Squares (CNRLS) method (11-15). Fitting was carried out using the software Thales-SIM (Zahner-Elektrik GmbH & Co. KG, Kronach, Germany) accepting a fitting error below 1% and relative uncertainty of each element lower than 30%. The equivalent circuit used for the fitting procedure (Figure 1) was used in a previous study with cells coming from the same batch (10).
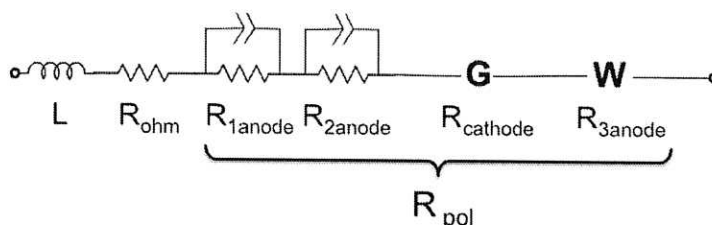

Figure 1. Equivalent circuit used for CNRLS fitting.

An inductive element (L) was used to model the respective contribution, at high frequencies, generally due to the wiring between the sample and the instrument. R_{ohm} represents the ohmic resistance, depending on the electrolyte and contacting losses. Its value is identified, in Nyquist plots, as the high-frequency intercept of the real part axis. Two resistance//constant phase element meshes (R_{1anode} and R_{2anode}) were used to fit the higher frequencies of the cell polarization (R_{pol}). They describe loss contributions related to the anode functional layer due to the gas diffusion, charge transfer and ionic transport in the bulk of the electrode. A Gerischer element was used to fit the medium frequency range characterized by the cathodic loss contributions ($R_{cathode}$). They include the surface exchange kinetics of oxygen and its ionic diffusivity within the bulk of the electrode. The low frequency part of the spectra was described by a bounded Warburg element modeling the gas diffusion impedance of the anode substrate (R_{3anode}).

After the preliminary electrochemical characterization held at open circuit voltage, cells were electrically loaded for 100 hours in galvanostatic mode applying a constant current necessary to lower the initial cell potential to 0.9 V. Once the OCV was stabilized after the removal of electric load, impedance spectra were recorded to evaluate the changes in the ohmic and cell polarization contributions.

Cells and interconnects were individually studied post-experiment. XRD analysis was performed on the cell cathode to evaluate the presence of pollutant compounds due to the interaction with the current collector. Sample cross-sections were prepared by mounting in epoxy resin, cutting and polishing with diamond suspensions up to 250 nm grain size. Such sections were observed and analyzed using a scanning electron microscope Zeiss Evo 40, equipped with EDX detector PentaFET.

The cathode contacting area of each sample was evaluated through image analysis (Fiji Imagej 1.47 h) on SEM micrographs.

Results

XRD analyses on LNF powders showed that already after the firing treatment at 600°C for four hours the right rhombohedral phase was formed (Figure 2). Each peak found in the diffraction profile matched the powder diffraction file 01-088-0637 of the $LaFe_{0.4}Ni_{0.6}O_{0.3}$. No additional peaks, due to unwanted phase formation or contaminations, were found.

The annealing treatments were applied to increase crystallinity, noticeable by sharper diffraction peaks. Fired powders were chosen for further processing to avoid the coarsening induced by the annealing treatment.

The CTEs reported in Figure 3 were calculated relative to the room temperature by the dilatometry data. LSCF exhibited the highest values, increasing the deviation from those of the other materials at 250 °C. LNF showed closer values and a similar behavior compared to the current collector material. Its CTE value resulted in between those of Crofer 22 APU and LSCF for the whole testing temperature range. It confirmed the possibility to use LNF as contacting layer between LSCF electrodes and Crofer 22 APU interconnect since its intermediate expansion would accommodate the thermal stresses between the two materials.
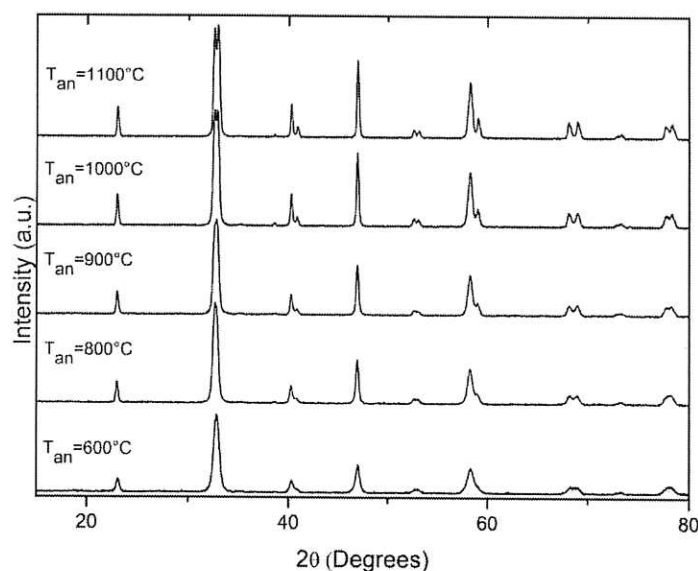
Figure 2. Diffraction profiles of LNF powders fired at 600°C and annealed in the range 800-1100°C.
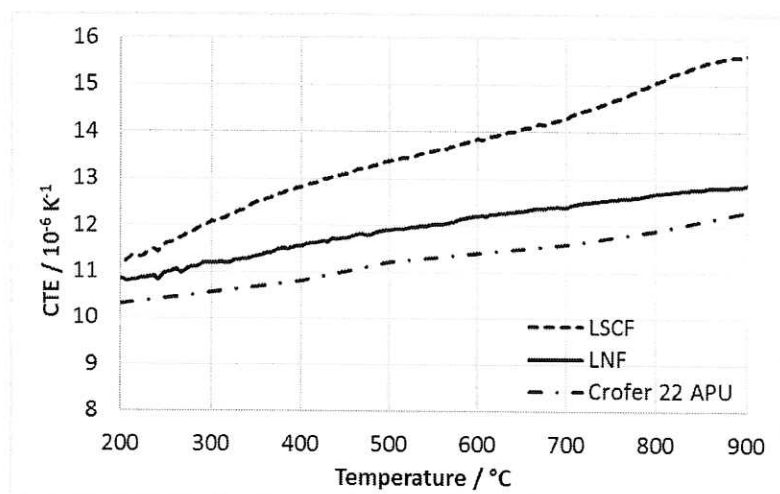

Figure 3. Temperature dependence of the coefficient of thermal expansion of LSCF and LNF compared to Crofer 22 APU (16).

The I-V curves measured at 750°C confirmed the influence of the contacting solution on the cell performances. As observed in a previous study (10), the use of a contacting material increases the cell power output by reducing the ohmic losses. In Figure 4 the effect of the cathode contacting layer addition is clearly visible in the mitigation of the slope in the voltage curve. Such optimization is due to the reduction of the ohmic losses in the cathode contacting region. The same effect was observed with the application of both LNF and LSCF. It consisted in the increase of the cell power at 0.7 V from 124 mW cm^{-2} to 640 mW cm^{-2} using LSCF and 577 mW cm^{-2} with LNF. The differences measured changing the contacting material can be attributed to variations in the contact area at the cathode side (Table I). The extension of the interconnect-contacting interface was lower due to the settlement of the contact layer after its application.
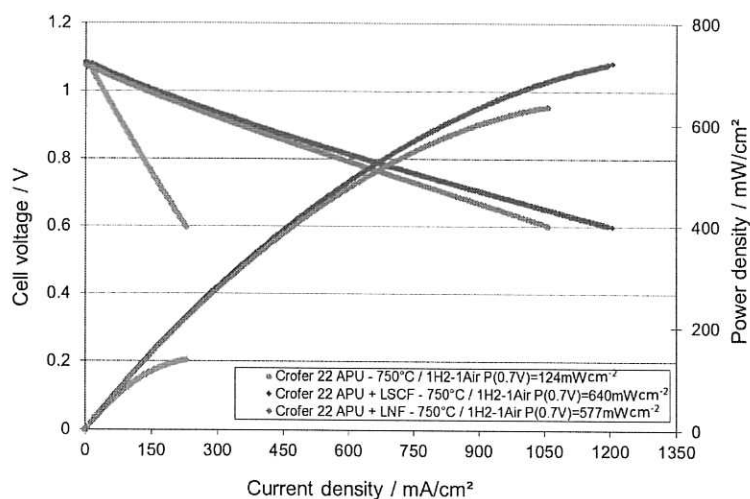
Figure 4. I-V curves and power densities of cells measured at 750°C, 1 Nlpm air at the cathode side and 1 Nlpm H_2 with 3 vol.% H_2O at the anode.

The impedance spectra exhibited similar total resistance and polarization contributions (Figure 5). The higher ohmic contribution measured with LNF confirmed the cause of the lower power output as previously hypothesized by the differences in the I-V curve slope.

The cell polarization was smaller as result of significantly lower gas diffusion impedance of the anode substrate (R_{3anode}). The other polarization contributions exhibited higher values. In particular, the cathode polarization was more than 30% higher when LNF was used as contact material. Such differences can be related to the influence of the ohmic losses to the cell polarization due to the uneven current distribution along the cell section (3,10).
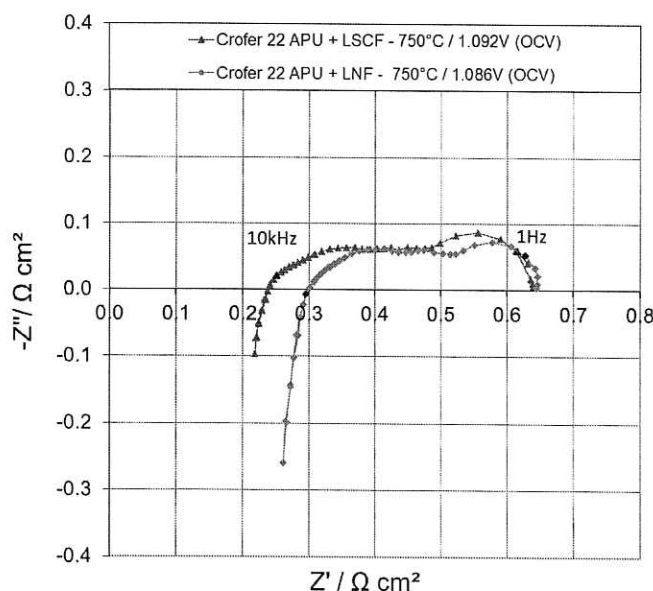

Figure 5. Impedance spectra of the cells contacted using Crofer 22 APU as cathodic current collector with LSCF and LNF contacting paste layers.

The galvanostatic load applied to the cells resulted in both cases in a linear decrease of their voltage. The cell contacted using LSCF started with a power output of 343 mW cm^{-2} at 0.9 V while with LNF it was 299 mW cm^{-2} (Table II). Keeping constant the current load, after 100 hours, the cell overpotential increased by 6 mV for the first cell and only 1 mV for the second one. Such variations consisted in a power output drop of 2 and 1 mW cm^{-2} respectively. Recording the impedance spectra before and after such test allowed investigating the source of the cell degradation (Table I).

TABLE I. Impedance contributions calculated by CNLS method before and after the galvanostatic test.

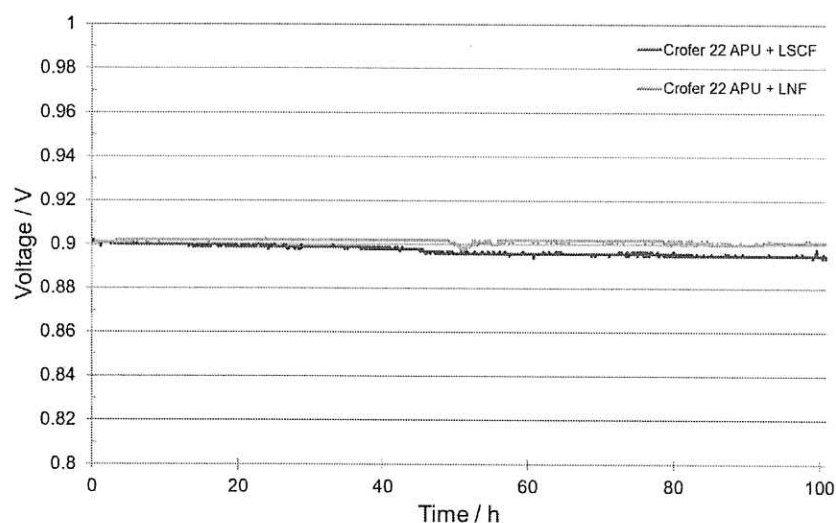| Sample	R_{ohm} / Ω cm^2	R_1+R_2 / Ω cm^2	$R_{cathode}$ / Ω cm^2	$R_{3\ anode}$ / Ω cm^2	$R_{polarization}$ / Ω cm^2	Cathode contacting Area / cm^2
LSCF – 0 h	0.239	0.139	0.075	0.187	0.401	10.02
LSCF – 100 h	0.240	0.118	0.026	0.196	0.340	
LNF – 0 h	0.299	0.173	0.100	0.075	0.348	2.51
LNF – 100 h	0.292	0.170	0.104	0.076	0.350	

Figure 6. Impedance spectra of the cells contacted using Crofer 22 APU as cathodic current collector with LSCF and LNF contacting paste layers.

TABLE II. Summary of the cell parameters before and after the galvanostatic test.

Sample	Overpotential / mV	Power density / mW cm^{-2}	Current density / mA cm^{-2}
LSCF – 0 h	193	343	381
LSCF – 100 h	199	341	
LNF – 0 h	181	299	332
LNF – 100 h	182	298	

The first cell improved its polarization impedance decreasing its resistive value by 61 mΩ cm^2. This change was due to the decrease of the R_1+R_2 and $R_{cathode}$ contributions that can be attributed to a better sintering of the electrodes as a result of the combined action of the operating temperature and the current. However, the increase of the ohmic contribution led to the power output decrease. The use of LNF as contact material ensured higher stability during the galvanostatic test. The impedance measurements revealed an increase by 2 mΩ cm^2 of the cell polarization. Also in this case, the R_1+R_2

contributions improved even if at lower extent compared to the previous cell. The cathode performance worsened measuring an increase of 4 mΩ cm^2. However, the decrease by 7 mΩ cm^2 of the ohmic resistance values compensated the reduced cell polarization contribution in terms of power output.

The XRD patterns measured on the cathode side of both cells were compared to those measured using Crofer 22 APU current collector without contact paste and only platinum mesh (Figure 7). This allowed distinguishing between the contributions of the cathode material, contacting and additional phases due to the presence of the FSS current collector.

All the peaks visible in the diffraction pattern of the cell contacted using a platinum mesh are attributed to the LSCF cathode material. The use of Crofer 22 APU as current collector at the cathode side gave rise to the presence of additional peaks ascribed to Cr, Mn and Fe based oxides.

When a contact layer was applied on the cathode side, the footprint of the current collector was visible on the electrode. It gave the possibility to acquire the XRD spectra on both the interconnect/electrode interface and under the interconnect channel. Similar patterns were recorded in both positions confirming the formation of the same compounds. This result highlighted the element migration phenomena via volatile species formation and precipitation within the electrode. Alloying elements of the FSS can also migrate by solid-state diffusion as already observed in previous studies (17-19).
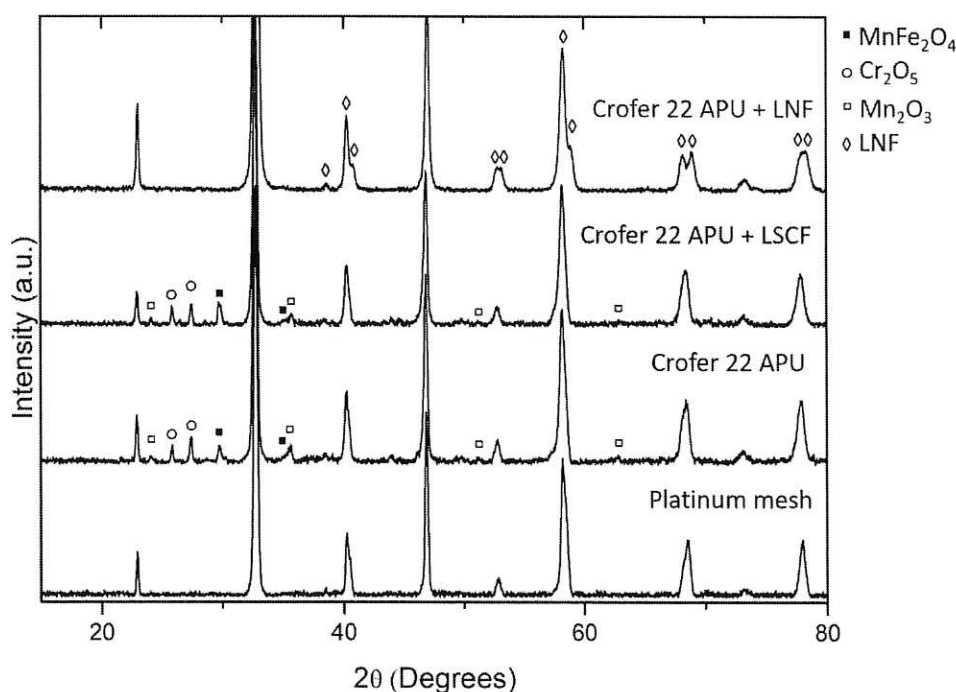

Figure 7. X-ray diffraction patterns of the cathode surface of the cell contacted with Crofer 22 APU with and without different contact layers. The diffraction patterns are compared with that measured on the cell contacted using platinum mesh only (17).

On the XRD pattern measured on the LNF contacted cell, additional peaks, related to the contact material were observed. In this case, no pollutant phases were detected at the cathode side. LNF is known as chromium tolerant cathode material (20-22) since the absence of strontium limits the formation of stable compounds based on such elements. However, the chromium migration by volatile species formation cannot be limited except by applying an additional *ad hoc* protective layer on the metal surface. Pollutants might be precipitated in localized areas of the electrode or in distributed not detected quantities.

In Figure 8 the interconnect-contact layer interfaces are shown for both samples. The current collector exhibited the formation of well adherent oxide layers, thicker when in contact with LSCF. The scale was mainly constituted by $Cr_{2-x}Fe_xO_3$ and $(Cr,Mn)_3O_4$. The formation of such oxide compounds at high temperatures on FSS is known to limit chromium evaporation and to be characterized by good electronic conductivity (17, 18, 23-28). Within the first μm of the LSCF contacting material a brighter region was also visible. It was attributed to the interaction between the two materials. In previous studies the LSCF characteristic was observed to interact with chromium being able to fix it on its surface forming secondary phases (29, 30). Additionally, the presence of a well-packed contact layer can be related to the lower R_{ohm} contribution. The measured evolution of such value can be due to the increase over time of the interconnect oxide layer thickness.

In the LNF contacted sample, the oxide scale on the interconnect was thinner and no interaction layer between the two materials was observed confirming the XRD results. The contact material looked more porous and constituted by particles with distributed sizes. These aspects could introduce higher ohmic losses as measured by EIS in comparison to the previous sample. Additionally, such morphology could evolve in denser layer due to the sintering for the combined temperature and current effects. It would result in the improvement of the contact resistance as observed in the reduction of the R_{ohm} contribution.
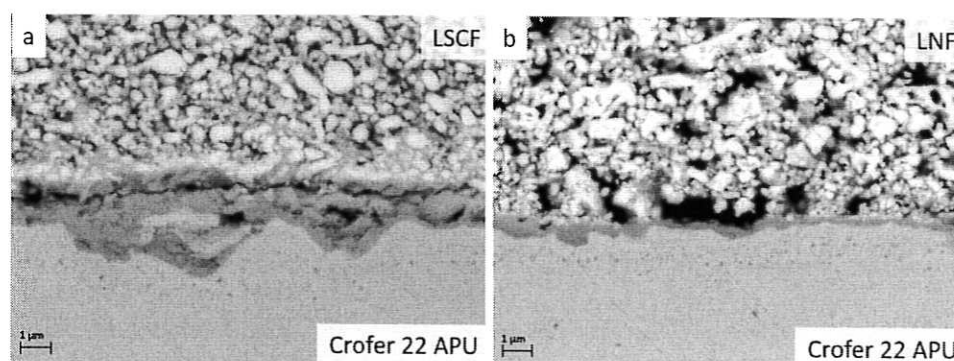

Figure 8. SEM-BSE images on cross-sections of the interconnect-contacting interfaces with (a) LSCF and (b) LNF.

Conclusions

In this work, LNF powders were synthesized by sol-gel method and used to produce a cathode contact ink. Such material exhibited CTE values between those of Crofer 22 APU and LSCF up to 900 °C. The effects of LNF and state-of-art LSCF contact inks on

ASCs were compared in terms of cell performances and degradation under current load. The use of LSCF resulted in lower ohmic losses. Despite the comparable total resistance of the two cells, higher power output was measured with LSCF contact material. This result confirmed the role of the ohmic losses in the overall cell performances affecting the power density to a greater extent compared to the cell polarization contributions.

The application of a constant current load resulted in a significant increase of the overpotential of the cell contacted with LSCF while the use of LNF ensured higher stability. This evolution was driven by changes in the R_{ohm} contributions, which increased in the first cell while decreased with LNF contacting.

The post-experiment investigations evidenced different extensions of the contacting interface in the two samples. Such aspect could have influenced the ohmic contributions. Microstructural differences were observed in the two contacting layers. LSCF was characterized by well-packed particles and the presence of an interaction Cr-rich layer while higher porosity was observed in LNF and no presence of unwanted phases.

The combination of electrochemical and post-experiment investigations highlighted the complex nature of the cathode contacting region. The effects of such layers on the cells are not fully predictable by the electrical and mechanical properties of the involved materials. The extension of the contact interface between the electrode and the current collector, interaction between coupled materials and microstructural changes resulted in critical factors influencing the measured power densities. Such aspects have to be taken into account, at the cell level, for proper comparison of performances considering the contacting effects on their measurement and evolution. Additionally, optimal contact materials and design have to be implemented in stacks to minimize losses in their power density.

Acknowledgments

References

1. S. P. Jiang, *J. Electrochem. Soc.*, **148**, A887 (2001).
2. Z. Yang, G. Xia, P. Singh and J. W. Stevenson, *J. Power Sources*, **155**, 246 (2006).
3. S. P. Jiang, J. G. Love and L. Apateanu, *Solid State Ion.*, **160**, 15 (2003).
4. K. Föger, R. Donelson and R. Ratnaraj, *Solid Oxide Fuel Cells (SOFC-VI)*, S.C. Singhal and M. Dokiya, Editors, **PV 99-19**, p. 95, The Electrochemical Society Proceedings Series, Pennington, NJ (1999).
5. M. C. Tucker, L. Cheng and L. C. DeJonghe, *J. Power Sources*, **196**, 8313 (2011).
6. X. Montero, F. Tietz, D. Stöver, M. Cassir and I. Villarreal, *J. Power Sources*, **188**, 148 (2009).

7. W.-J. Shong, C.-K. Liu, C.-W. Lu, S.-H. Wu and R.-Y. Lee, *Int. J. Hydrogen Energy* **42**, 1170 (2017).
8. S. P. Simner, J. F. Bonnet, N. L. Canfield, K. D. Meinhardt, V. L. Sprenkle and J. W. Stevenson, *Electrochem. Solid State Lett.,* **5**, A173 (2002).
9. L. Millar, H. Taherparvar, N. Filkin, P. Slater and J. Yeomans, *Solid State Ion.,* 179, **732** (2008).
10. R. Spotorno, P. Piccardo and G. Schiller, *J. Electrochem. Soc.,* **163** (8) F1-F5 (2016)
11. B. A. Boukamp, *Solid State Ion.,* **20**, 31 (1986).
12. J. R. Macdonald and L. D. Potter, *Solid State Ion.,* **24**, 61 (1987).
13. D. W. Marquardt, *J. Soc. Ind. Appl. Math.* **11**, 431 (1963).
14. K. Levenberg, *Q. Appl. Math.,* **2**, 164 (1944).
15. C. Comminges, Q. X. Fu, M. Zahid, N. Y. Steiner and O. Bucheli, *Electrochim. Acta*, **59**, 367 (2012).
16. VDM® Crofer 22 APU Material Data Sheet No. 4046 May 2010 Edition, VDM Metals.
17. R. Spotorno, P. Piccardo and G. Schiller, *ECS Trans*, **68**, 2429 (2015).
18. R. Spotorno, P. Piccardo and F. Perrozzi, *ECS Trans*, **68**, 1633 (2015).
19. S. P. Jiang and X. Chen, *Int. J. Hydrogen Energy*, 39, 505 (2014).
20. T. Komatsu, H. Arai, R. Chiba, K. Nozawa, M. Arakawa and K. Sato, *J. Electrochem. Soc.* 154 (2007) B379
21. A. Morán-Ruiz, K. Vidal, M. Á. Laguna-Bercero, A. Larrañaga and M. I. Arriortua, *J. Power Sources* 248 (2014) 1067
22. G. Y. Lau, M. C. Tucker, C. P. Jacobson, S. J. Visco, S. H. Gleixner and L. C. De Jonghe, *J. Power Sources* 195 (2010) 7540
23. P. Piccardo, S. Anelli , V. Bongiorno, R. Spotorno, L. Repetto and P. Girardon, *Int. J. Hydrogen Energy*, **40**, 3726 (2015).
24. Z. Yang, J.S. Hardy, M.S. Walker, G. Xia, S.P. Simner and J. W. Stevenson, *J. Electrochem. Soc.,* **151**, A1825 (2004).
25. T. Horita, H. Kishimoto, K. Yamaji, Y. Xiong, N. Sakai, M. E. Brito and H. Yokokawa, *J. Electrochem. Soc.,* **153**, A2007 (2006)
26. V. Miguel-Pérez, A. Martínez-Amesti, M. L. Nó, A. Larrañaga and M. I. Arriortua, *Corros. Sci.,* **60**, 38 (2012).
27. K. Kawamura, T. Nitobe, H. Kurokawa, M. Ueda and T. Maruyama, *J. Electrochem. Soc.,* **159**, B259 (2012)
28. M. Linder, T. Hocker, L. Holzer, K. A. Friedrich, B. Iwanschitz, A. Mai and J. A. Schuler, *J. Power Sources,* **243**, 508 (2013).
29. T. Horita, D. H. Cho, F. Wang, M. Nishi, T. Shimonosono, H. Kishimoto, K. Yamaji, M. E. Brito and H. Yokokawa, *ECS Transactions*, **51**, 69 (2013).
30. Grace Y. Lau, Michael C. Tucker, Craig P. Jacobson, Steven J. Visco, Stacy H. Gleixner and L. C. DeJonghe, *J. Power Sources,* **195**, 7540 (2010).